https://doi.org/10.5194/egusphere-2026-4742
Preprint. Discussion started: 2 September 2026

Episodic Neoproterozoic Magmatism in the Northeastern Yangtze Craton: Implications for the Breakup of the Rodinia Supercontinent

Shengzhu Wang[1], Huaiyu Yang[2], Xiaoyu Yuan[3]

[1]Shandong Institute of Petroleum and Chemical Technology, Dongying 257061, China.
[2]Exploration and Development Research Institute of Shengli Oilfield Company, Sinopec, Dongying 257015, China.
[3]Frontiers Science Center for Deep Ocean Multispheres and Earth System, Key Laboratory of Submarine Geosciences and Prospecting Techniques, Ministry of Education and College of Marine Geosciences, Ocean University of China, Qingdao 266100, China.

Correspondence to: Xiaoyu Yuan (yuanxiaoyu@ouc.edu.cn)

Abstract. The composition and evolution of Precambrian basement are pivotal for understanding global continental crustal growth and supercontinent cycles, representing a key frontier in geological research. Although ancient basement exposures have been documented along the periphery of the Yangtze Craton, its northern margin exhibits limited and sporadic Precambrian outcrops, resulting in poorly constrained crustal evolution history for this critical period. This study identifies a series of magmatic rocks with mid-Neoproterozoic ages along the northeastern margin of the Yangtze Craton, which provides new constraints on the tectonic evolution of the Yangtze Craton in Neoproterozoic. This discovery provides critical constraints on the crystalline basement attributes and tectonic evolution during this stage, while offering vital evidence for investigating its linkage with the Rodinia supercontinent. Geochronological results reveal two magmatic episodes: 781–776 Ma granitic gneisses (Feidong Complex) and 753–730 Ma bimodal volcanic rocks (spilite-keratophyre association; Zhangbaling Group). Contrasting geochemical signatures and isotopic compositions indicate complex melting conditions and tectonic stages: the Feidong granitic gneisses exhibit highly enriched zircon Lu-Hf isotopes ($\varepsilon_{Hf}(t)$ = −16.9 to −10.9) and ancient crustal model ages, attesting to remelting of ancient continental material, elevated Sr/Y, $(La/Yb)_n$ ratios coupled with significantly fractionated REE patterns showing significant HREE depletion imply high-pressure melting conditions. During this phase, decompression melting of the lithospheric mantle occurred, inducing lower crustal melting via underplating. In contrast, the Zhangbaling bimodal volcanics display diagnostic A-type granite geochemical affinities, depleted zircon Lu-Hf isotopes ($\varepsilon_{Hf}(t)$ = −3.9 to +4.3), and shallower melting depths. This upward shift in magmatic source records the transition of the northeastern Yangtze margin from initial extension to a mature rift system, directly recording the Rodinia supercontinent breakup process.

1 Introduction

McMenamin and McMenamin (1990) systematically reconstructed two Neoproterozoic continental blocks—East Gondwana and West Gondwana—based on tectonic belt data from the 1970s–1980s, proposing their derivation from the breakup of a Precambrian supercontinent designated Rodinia. Subsequent integration of geological records with paleomagnetic data by

https://doi.org/10.5194/egusphere-2026-4742
Preprint. Discussion started: 2 September 2026

Dalziel (1991), Hoffman (1991), and Moores (1991) established a comprehensive reconstruction model for this supercontinent. Rodinia is widely accepted to have assembled through global-scale Grenvillian orogeny (1.3–0.9 Ga), with its fragmentation driven by mantle upwelling beneath the supercontinent (Moores, 1991; Li et al., 2008). This rifting initiated at 850–830 Ma (Li et al., 1999, 2008, 2012; Xia et al., 2012) and culminated at 600–540 Ma (Li et al., 2008; Xia et al., 2012).

Recent researches have focused on Neoproterozoic magmatism associated with Rodinia's assembly and breakup along the Yangtze periphery. The southeastern margin (exemplified by Jiangnan Orogen) features early Neoproterozoic island-arc (e.g., Shuangxiwu magmatic arc) or active continental margin calc-alkaline suites (Wu et al., 2006; Zheng et al., 2007, 2008; Li et al., 2009; Zhao et al., 2011; Zhang et al., 2012; Xu et al., 2014; Yang et al., 2015), accompanied by 825–815 Ma S-type granite intrusions (Li et al., 1999; Zhao et al., 2013a)—a period broadly regarded as marking the final Yangtze-Cathaysia amalgamation. These basement rocks are unconformably overlain by the Nanhua Basin strata (e.g., Banxi Group), which contain minor 815–750 Ma A-type granites and bimodal volcanic rocks (Zhao, 2015). Along the western margin (Panzhihua-Hannan zone), magmatic activity comprises mainly 1000–750 Ma calc-alkaline intrusives (Zhao and Zhou, 2008) with subsidiary 825–750 Ma bimodal magmatism and A-type granite. Isotopic signatures indicate dominant remelting of late Mesoproterozoic-early Neoproterozoic juvenile crust, reflecting prolonged oceanic subduction-controlled crustal accretion during Rodinia assembly. Notably, the local emergence of low-$\delta^{18}O$ magmas from ca. 820 Ma marks incipient back-arc extension (Zhang and Zheng, 2013). The northern margin preserves Rodinia-related magmatic records within the Kongling Complex, including the late Mesoproterozoic Miaowan ophiolite suite (1115–1100 Ma), forearc mafic rocks (1000–970 Ma; Deng et al., 2017), and 940–930 Ma metamorphic events (Jiang et al., 2016). Conversely, 860–790 Ma mafic dikes and ancient crust-derived granites formed under regional extension (Zhang et al., 2009; Wei et al., 2012; Zhao et al., 2013a, b). These records collectively demonstrate pronounced spatial heterogeneity in Neoproterozoic magmatism along the Yangtze periphery, indicative of distinct regional tectonic settings and evolutionary histories.

Previous studies have reported Neoproterozoic magmatic rocks along the northeastern margin of the Yangtze Craton, but their geodynamic significance have not yet been systematically clarified. In this study, we identify and characterize Neoproterozoic magmatic sequences in this region to provide tighter constraints on its tectonic evolution. Through integrated field investigations, petrographic analysis, geochemistry, zircon U-Pb chronology, and in-situ Lu-Hf isotopes, we establish precise emplacement ages, characterize source attributes and magmatic differentiation processes, and elucidate petrogenetic mechanisms and evolutionary trends. These magmatic records not only provide critical constraints on the extensional processes, geodynamic mechanisms, and tectonic evolution of the study area but also furnish key evidence for reconstructing the Neoproterozoic structural evolution history of the entire Yangtze Craton.

2 Geological setting

The Triassic collision of the South China Block with the North China Block resulted in both the Dabie-Sulu orogenic belt and its synchronously developed NNE-trending Tan-Lu Fault Zone (TLFZ) (Zheng et al., 2003; Zhu et al., 2005, 2010, 2018).

https://doi.org/10.5194/egusphere-2026-4742
Preprint. Discussion started: 2 September 2026

Along the eastern boundary of TLFZ, the Zhangbaling Uplift displays a low-grade metamorphic unit, contrasting sharply with adjacent high- to ultrahigh-pressure metamorphic belts. This uplift preserves Paleoproterozoic to Neoproterozoic basement rocks, comprising the northern Zhangbaling Group and southern Feidong Complex (Cai et al., 2021; Yuan et al., 2021, 2022a, b, 2024). Its western margin borders the Hefei Basin, while the eastern limit transitions into a foreland deformation belt, overlain by Sinian to Triassic sedimentary cover.

The Feidong Complex, exposed over ~240 km ^{2} in the southern Zhangbaling Uplift (Fig. 1), contacts the northern Zhangbaling Group via fault. Based on petrographic and microstructural analyses, this complex is divided into four tectono-lithostratigraphic units from base to top: 1) Fuchashan Unit (monzonitic gneiss, amphibole-plagioclase gneiss); 2) Dahengshan Unit (biotite-plagioclase gneiss, quartz schist); 3) Shuangshan and Qiaotouji Units (phosphorus-bearing marble, biotite schist) (Kang et al., 2013). Inter-unit contacts are predominantly gradational. Influenced by intense Early Cretaceous TLFZ activity, rocks underwent pervasive ductile deformation and lower amphibolite-facies metamorphism with peak pressures of 0.5–0.9 GPa and temperatures of 524–650 ℃ (Kang et al., 2013; Nie et al., 2015; Shi et al., 2016).

The Zhangbaling Group (Fig. 1) primarily outcrops along the eastern TLFZ flank within northern and local southern sections of the Zhangbaling Uplift, with minor exposure along the southeastern Dabie orogen. This group consists of the Xileng and Beijiangjun formations representing a marine volcanic-sedimentary association dominated by quartz-keratophyre with subordinate spilite, volcaniclastic rocks, and tuffaceous sediments, intercalated with siliceous rocks, dolomitic limestone lenses, siltstone, and shale. The Xileng Formation consists of interlayered greenschist-facies metamorphosed mafic-felsic alkaline volcanics and clastic rocks (Liou et al., 1992; Zhang et al., 2007). Protoliths are dominated by quartz-keratophyre followed by keratophyre and spilite (Guo et al., 1995), metamorphosed under medium- to high-greenschist facies (Zhang et al., 2007). It exhibits distinct eruptive-effusive-sedimentary cycles with rare effusive porphyritic quartz-keratophyre, abundant eruptive-effusive transitional quartz-keratophyric tuff/tuff-lava, and sedimentary interbeds of mudstone/siltstone during volcanic quiescence. The Beijiangjun Formation is a 400-m-thick, low-greenschist facies metasedimentary sequence comprising (base to top) marble, crystalline limestone, metamorphic siltstone, and phyllite, derived from mudstone-siltstone protoliths. Muscovite $^{40}Ar/^{39}Ar$ dating indicates deformation and metamorphism occurred predominantly during the Middle Triassic, synchronous with orogen-parallel TLFZ activity (Zhao et al., 2014).

https://doi.org/10.5194/egusphere-2026-4742
Preprint. Discussion started: 2 September 2026

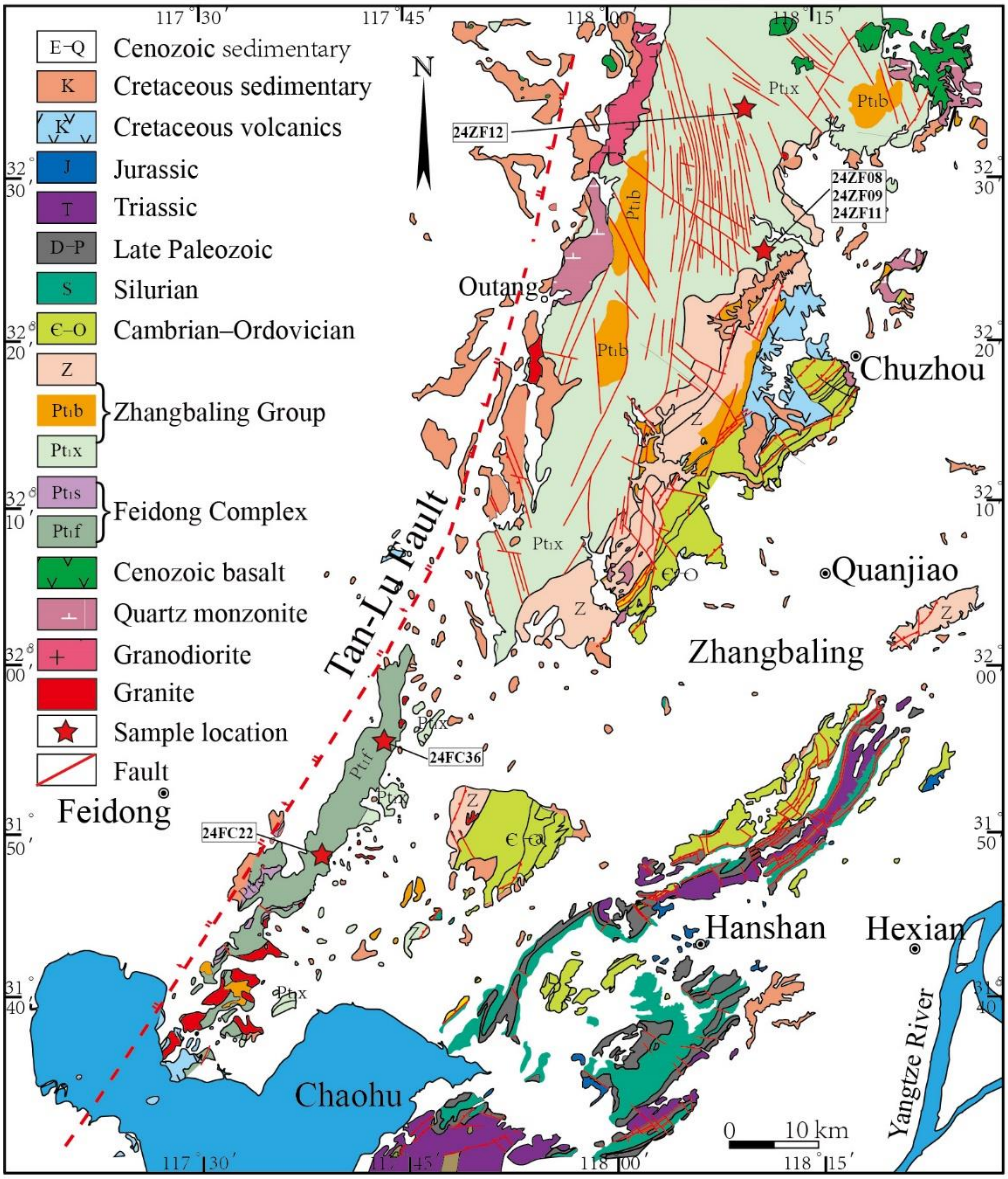

Figure 1: Sketch geological map of the Zhangbaling Uplift segment and sample locations.

90 ## 3 Sample description

Field sampling targeted the Xileng Formation (Zhangbaling Group) and Feidong Complex, comprising granitic gneiss of the Feidong Complex, alongside quartz keratophyre and spilite from the Xileng Formation. Outcrops range from 10 to 30 m in length and exhibit generally low weathering intensity.

https://doi.org/10.5194/egusphere-2026-4742
Preprint. Discussion started: 2 September 2026

Petrographic analysis reveals that the granitic gneiss (Fig. 2e, f) displays medium-grained granoblastic texture with gneissose structure. Mineral assemblages consist of porphyroclasts dominated by quartz (25–35%), plagioclase (20–30%), K-feldspar (15–25%), and biotite (5–10%), set in a finer-grained matrix with accessory apatite and titanite. Pronounced mineral preferred orientation is evident. Plagioclase and K-feldspar porphyroclasts exhibit euhedral to subhedral shapes (0.2–0.5 mm) bordered by irregular quartz overgrowths. Quartz occurs as subhedral to anhedral grains (0.1–0.3 mm), while biotite forms acicular or bladed crystals (0.1–0.3 mm) aligned parallel to the foliation.

The quartz keratophyre (Fig. 2g, h) exhibits porphyritic texture with relict trachytic fabric. Phenocrysts comprise oriented plagioclase (15–20%) and quartz (20–25%), embedded in a groundmass dominated by quartz microcrysts (45–50%) and minor anhedral muscovite. Plagioclase phenocrysts are extensively argillized by alteration, with rare albite twins observed. Quartz microcrysts surround phenocrysts, defining vestigial flow structures.

The spilite sample (Fig. 2i, j) characteristically displays spilitic texture with amygdaloidal structure. Primary mineral assemblages include feldspar (35–40%), pyroxene (25–30%), and quartz (10–15%), with secondary chlorite and epidote. Subhedral to anhedral feldspar (0.5–1 mm), aligned in bundled aggregates, shows serrated margins and skeletal texture wherein cavities are infilled by glass, flocculent pyroxene, and alteration products. Anhedral pyroxene grains (0.2–0.5 mm) occupy interstitial spaces within feldspar frameworks. Anhedral quartz (0.05–0.3 mm) exhibiting undulatory extinction fills residual voids in the mineral framework.

https://doi.org/10.5194/egusphere-2026-4742
Preprint. Discussion started: 2 September 2026

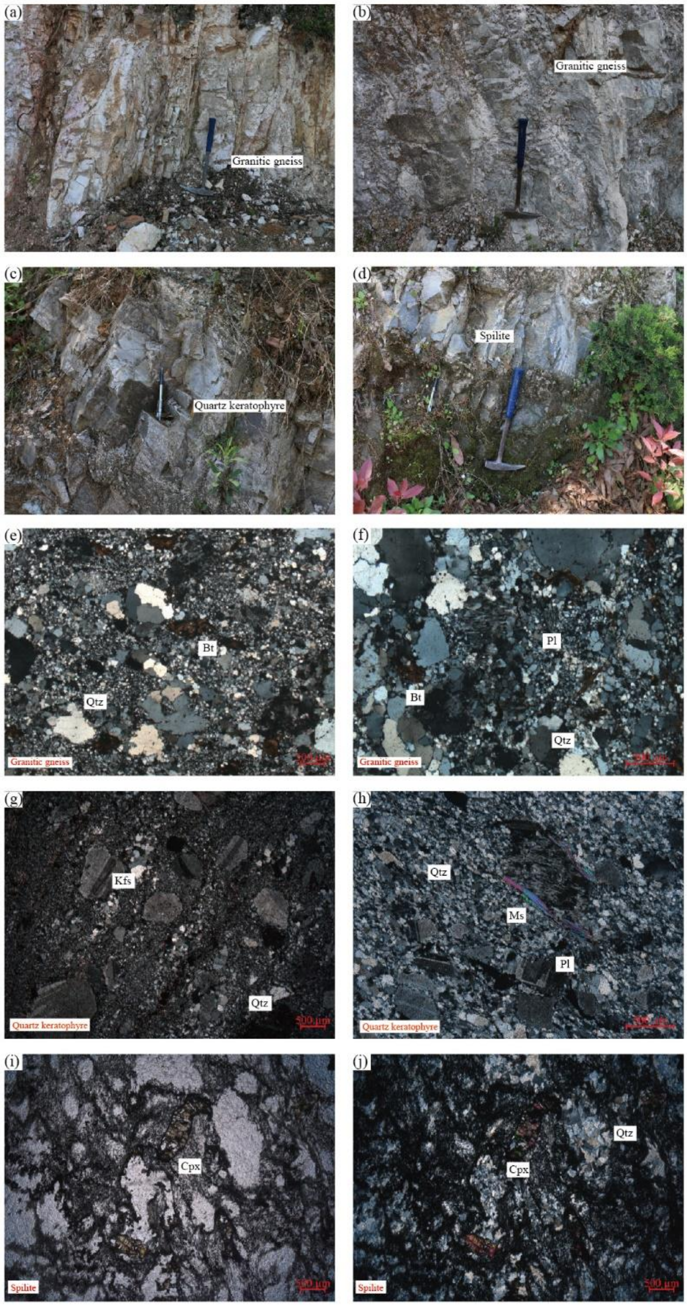

Figure 2: Representative field photographs and photomicrographs of representative samples from the Zhangbaling Uplift. Pl = plagioclase; Qtz = quartz; Bt = biotite; Ms = muscovite; Kfs = alkali feldspar; Cpx = clinopyroxene.

https://doi.org/10.5194/egusphere-2026-4742
Preprint. Discussion started: 2 September 2026

4 Analytical methods

Rock samples were collected from fresh outcrops exceeding 10 m^2 exposure area. During sample preparation, surface-weathered portions were removed before selecting petrographically representative sections for thin section fabrication. We performed zircon separation at Hebei Institute of Regional Geological and Mineral Survey (Langfang): Fresh samples for geochronology were jaw-crushed, with zircon concentrates obtained via conventional gravity and electromagnetic selection methods. Intact euhedral zircons were hand-selected, embedded in thermosetting resin, and section-polished to reveal internal cores. Analytical spots were targeted based on reflected/transmitted light and cathodoluminescence (CL) imaging.

4.1 LA-ICP-MS zircon U–Pb dating

At Wuhan SampleSolution (WSSAT), zircon U-Pb analyses utilized an Agilent 7700x ICP-MS connected to a 193 nm ArF excimer laser. The helium-based carrier system (0.8 L/min), supplemented with 0.03 L/min argon via T-connector, delivered aerosols to the ICP. Standardization involved zircon 91500 for U-Pb fractionation and NIST SRM 610 for trace elements. Data processing used ICPMSDataCal 9.0, with Concordia plotting and age calculations in Isoplot 4.11 (Ludwig, 2003), adhering to Zong et al. (2017).

4.2 Whole-rock major and trace-elements

A wavelength-dispersive XRF spectrometer (PANalytical Axios) at GPMR Lab (Shandong University of Science and Technology) measured major elements in borate-fused glass disks (sample:flux = 1:5; Pt crucible; 1150–1250 ℃), achieving sub-1% RSD reproducibility. High-resolution ICP-MS (Thermo Element 2) determined trace and REE abundances: 50 mg aliquots digested in sealed PTFE vessels with HF-HNO_3 (3:1) at 140°C for 48 hr, followed by $HClO_4$ addition and evaporation for fluorine removal. Residues were dissolved in 5% HNO_3 to 50 mL final volume, with analytical uncertainty <5% (2σ) for most elements.

4.3 Zircon Lu–Hf isotopes

A Neptune Plus multi-collector ICP-MS hosted at Shandong University of Science and Technology facilitated in situ zircon Hf isotopic measurements. Ablation utilized a Teledyne Cetac Analyte Excite laser (5.3 J/cm^2 energy density, 42 μm spot size, single-point mode) with He carrier gas (0.8 L/min) mixed with 3 mL/min N_2 to enhance sensitivity. International reference material 91500 was analyzed concurrently: 91500 standardized external correction (yielding $^{176}Hf/^{177}Hf$ = 0.282302±8, 2SD; consistent with solution values). Offline processing employed ICPMSDataCal 10.0.

https://doi.org/10.5194/egusphere-2026-4742
Preprint. Discussion started: 2 September 2026

5 Analytical Results

5.1 LA-ICP-MS zircon U–Pb ages

Zircon U-Pb geochronological results for Neoproterozoic granitic gneiss, quartz keratophyre, and spilite samples from the Zhangbaling Uplift are compiled in Sect. S1. Corresponding analytical pit locations documented by CL imagery appear in Fig. 3.

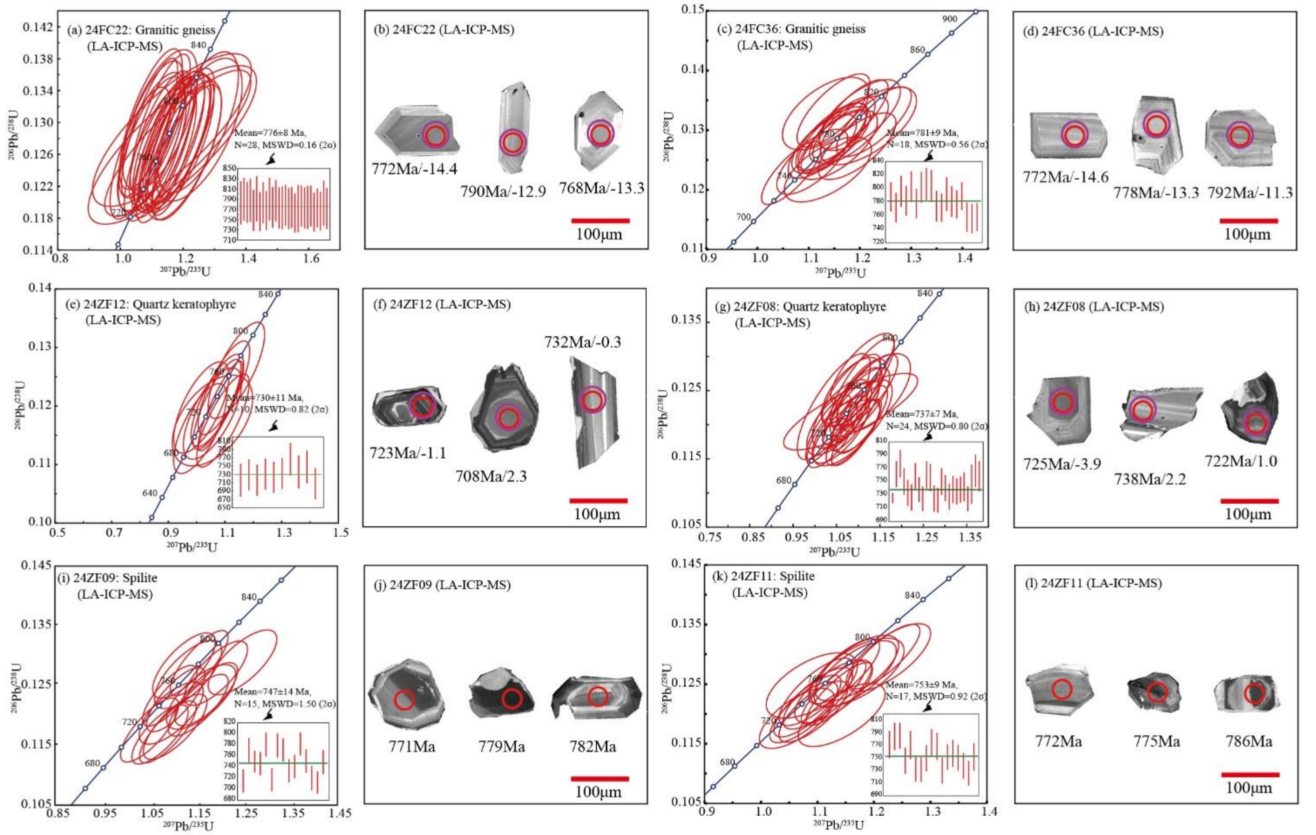

Figure 3: Typical cathodoluminescence (CL) images, zircon U-Pb concordia diagrams and weighted mean of $^{206}Pb/^{238}U$ ages of the Zhangbaling Uplift rock samples.

Granitic gneiss sample 24FC22 contains dominantly colorless to pale yellow, euhedral prismatic zircon grains (100–250 μm; 1:1–3:1 axial ratios), exhibiting magmatic oscillatory zoning in CL images, without metamorphic overgrowths. Twenty-eight spot analyses (>90% concordance) yield a coherent $^{206}Pb/^{238}U$ age spanning 791–763 Ma, with a weighted mean of 776 ± 8 Ma (MSWD = 0.16, n = 28), interpreted as the emplacement age (Fig. 3a, b).

Granitic gneiss sample 24FC36 displays euhedral to subhedral zircons (aspect ratios 1.5:1–3:1) exhibiting well-developed oscillatory zoning in CL. Eighteen analytical spots define a tight $^{206}Pb/^{238}U$ ages cluster (807–756 Ma), defining a weighted crystallization age of 781 ± 9 Ma (MSWD = 0.56; Fig. 3c, d).

https://doi.org/10.5194/egusphere-2026-4742
Preprint. Discussion started: 2 September 2026

Quartz keratophyre sample 24ZF12 comprises predominantly euhedral elongated prisms (50–200 µm; aspect ratios 1:1–4:1) exhibiting densely spaced oscillatory zoning. Ten concordant analyses define a clustered $^{206}Pb/^{238}U$ age population of 766-708 Ma and constrain the age of the volcanic eruption to 730 ± 11 Ma. (Fig. 3e, f).

Quartz keratophyre sample 24ZF08 contains mostly euhedral to subhedral zircon grains (70–200 µm; aspect ratios 2:1–3:1) with pronounced oscillatory zoning without obvious core-rim structure. Twenty-four spots reveal a continuous $^{206}Pb/^{238}U$ age spectrum from 777 to 722 Ma, producing a weighted mean crystallization age of 737 ± 7 Ma (MSWD = 0.80, 2σ; Fig. 3g, h).

Spilite sample 24ZF09 features euhedral to subhedral zircon crystals (50–120 µm; aspect ratios 1:1–1.5:1), exhibiting sector zoning and narrow grayish-white metamorphic overgrowths in CL images. Fifteen analyses give $^{206}Pb/^{238}U$ ages spanning 782–712 Ma, with a weighted mean of 747 ± 14 Ma (MSWD = 1.50, 2σ), constraining the magmatic crystallization age (Fig. 3i, j).

Spilite sample 24ZF11 contains colorless to pale yellow, euhedral prismatic zircons (50–150 µm; aspect ratios 1:1–2:1). Broad oscillatory zoning without core-rim texture in CL images. Seventeen analytical spots define a tight $^{206}Pb/^{238}U$ ages cluster (786–726 Ma), with a weighted mean of 753 ± 9 Ma (MSWD = 0.92, 2σ; Fig. 3k, l).

5.2 Major and trace element data

Six granitic gneisses from the Feidong Complex, six quartz keratophyres and four spilites from the Xileng Formation were analyzed for whole-rock major and trace elements. The results are presented in Sect. S2.

Granitic gneisses exhibit high SiO_2 (71.64–74.24 wt%), elevated total alkalis ($Na_2O + K_2O$ = 8.37–9.08 wt%), but depleted mafic components (MgO: 0.14–0.21 wt%; FeO^T: 1.83–3.13 wt%). Classified as high-K calc-alkaline granites on K_2O-SiO_2 diagram (Fig. 4b), they consistently plot in the subalkaline field of TAS (Fig. 4a) and exhibit weakly peraluminous character (A/CNK = 1.07–1.14; Fig. 4c). Total rare earth element (REE) distributions reveal light REE (LREE)-enriched patterns [$(La/Yb)_n$ = 19.84–44.44] with ∑REE = 144–393 ppm and moderate Eu anomalies (Eu/Eu* = 0.69–0.80; Fig. 5a). Primitive mantle-normalized spidergrams (Fig. 5b) show pronounced large-ion lithophile elements (LILE: Cs, Rb, Ba, K) and Zr-Hf enrichments coupled with HFSE (Nb, Ta, Ti) depletions, diagnostic of continental crustal rocks. Pronounced LREE/HREE fractionation and high Sr/Y ratios (24.68–37.68) suggest garnet stability in the source region.

https://doi.org/10.5194/egusphere-2026-4742
Preprint. Discussion started: 2 September 2026

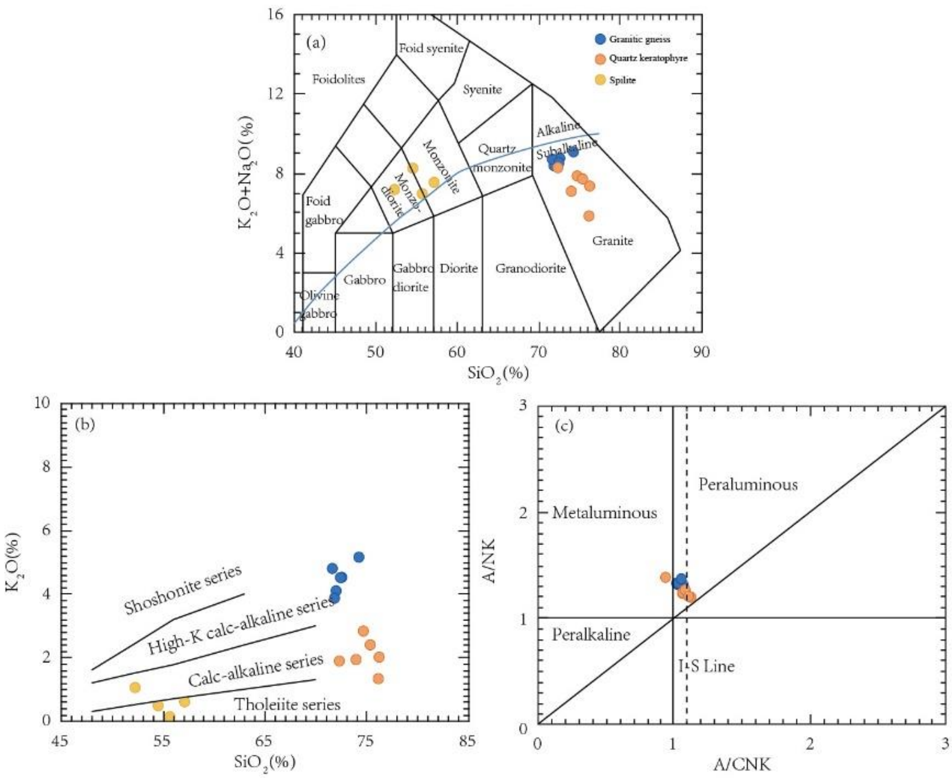

Figure 4: Plots of chemical compositions for the rock samples from the Zhangbaling Uplift. (a) Total alkali vs. SiO_2 (TAS) diagram; (b) SiO_2 vs. K_2O diagram; (c) A/CNK vs A/NK diagram.

Quartz keratophyres display high SiO_2 (72.33–76.24 wt%), Na_2O (4.55–6.42 wt%), and Al_2O_3 (11.58–15.02 wt%) concentrations but low K_2O (1.30–2.81 wt%) and MgO (0.10–0.21 wt%). Geochemical classification positions these samples predominantly in the subalkaline granite sector of the TAS diagram (Fig. 4a), exhibiting weak to moderate peraluminosity (A/CNK = 1.05–1.10; Fig. 4c). Total REE abundances (82–179 ppm) show enriched LREE and HREE depletion ($(La/Yb)_N$ = 1.50–8.96), with seagull-shaped patterns accentuated by Eu depletion (Eu/Eu* = 0.34–0.66), indicating plagioclase fractionation/residual phases (Fig. 5a). Primitive mantle-normalized spidergrams (Fig. 5b) exhibit LILE (Cs, Rb, Ba, K) enrichment, positive Zr-Hf anomalies, and HFSE (Nb, Ta, Ti) depletions, demonstrating crustal rocks.

Spilites are characterized by low SiO_2 (52.24–57.11 wt%), K_2O (0.10–1.02 wt%), CaO (3.95–5.31 wt%), TiO_2 (1.09–1.36 wt%), with K_2O/Na_2O (0.01–0.17), but high $Mg^{\#}$ (41.87–48.97), Na_2O (6.15–7.80 wt%), MgO (3.96–5.32 wt%), and Al_2O_3 (13.39–17.06 wt%). In the TAS classification scheme (Fig. 4a), the majority of specimens occupy the monzodiorite-monzonite compositional field, manifesting distinct alkaline geochemical affinity. Total REE concentrations (69–137 ppm) feature subtle LREE enrichment relative to HREE, evidenced by $(La/Yb)_n$ ratios of 3.37–3.73. Europium anomalies remain statistically insignificant (Eu/Eu* = 0.89–1.19; Fig. 5c). Primitive mantle-normalized trace element distributions (Fig. 5d) characterize by

https://doi.org/10.5194/egusphere-2026-4742
Preprint. Discussion started: 2 September 2026

significant LILE (Rb, Ba, Pb, K) enrichments and pronounced HFSE (Nb, Ta) depletions, exhibiting arc-type signatures indicative of non-asthenospheric mantle sources.

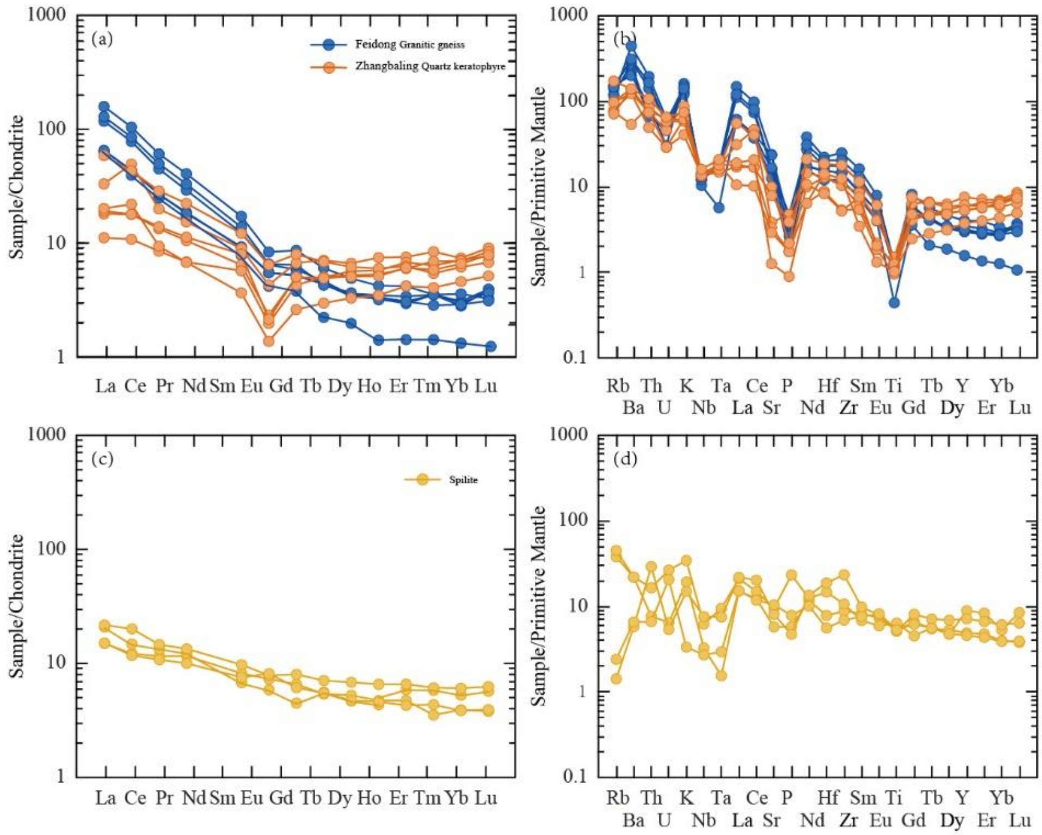

Figure 5: Chondrite-normalized rare earth element patterns (a, c) and primitive mantle normalized multi-element profiles (b, d) of the samples. Chondrite and primitive mantle normalizing values are from Boynton (1984) and Sun and McDonough (1989), respectively.

5.3 Zircon Lu–Hf isotopes

Zircon Lu-Hf isotopic analyses were conducted on two representative granitic gneiss samples and two quartz keratophyre samples, with results presented in Sect. S3.

Granitic gneiss sample 24FC22 yielded 15 analytical spots exhibiting $^{176}Lu/^{177}Hf$ ratios of 0.000818–0.004225 and $^{176}Hf/^{177}Hf$ ratios of 0.281860–0.282039. The corresponding $\varepsilon_{Hf}(t)$ values range from –16.4 to –10.6, with single-stage Hf model ages (T_{DM1}) of 2.03–2.01 Ga and two-stage model ages (T_{DM2}) of 2.70–2.34 Ga (Fig. 6).

Granitic gneiss sample 24FC36 (12 spots) displays $^{176}Lu/^{177}Hf$ = 0.001073–0.003075 and $^{176}Hf/^{177}Hf$ = 0.281840–0.281988. Calculated $\varepsilon_{Hf}(t)$ values (–16.9 to –11.3) correspond to T_{DM1} = 2.10–1.83 Ga and T_{DM2} = 2.750–2.40 Ga, referenced to their U-Pb crystallization ages (Fig. 6).

https://doi.org/10.5194/egusphere-2026-4742
Preprint. Discussion started: 2 September 2026

Quartz keratophyre sample 24ZF12 (10 spots) shows $^{176}Lu/^{177}Hf$ = 0.001289–0.003336 and $^{176}Hf/^{177}Hf$ = 0.282217–0.282440. These yield $\varepsilon_{Hf}(t)$ values of –3.1 to 2.3, with T_{DM1} = 1.45–1.22 Ga and T_{DM2} = 1.83–1.48 Ga (Fig. 6).

Quartz keratophyre sample 24ZF08 (14 spots) exhibits $^{176}Lu/^{177}Hf$ ratios spanning 0.002284–0.005689 and $^{176}Hf/^{177}Hf$ = 0.282256–0.282468. Resulting $\varepsilon_{Hf}(t)$ values range from –3.9 to 4.3, corresponding to T_{DM1} = 1.57–1.19 Ga and T_{DM2} = 1.91–1.40 Ga (Fig. 6).

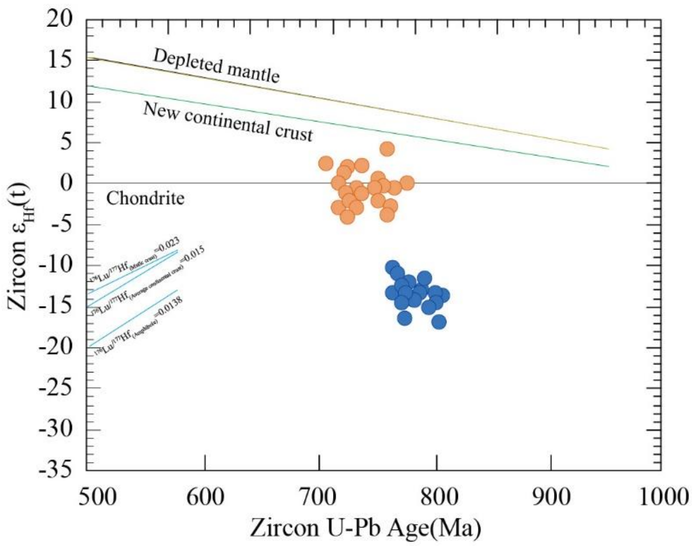

Figure 6: Hf isotope evolution diagram for samples from the Zhangbaling Uplift.

6 Discussion

6.1 Petrogenesis of Feidong granitic gneiss

Neoproterozoic granitic gneisses from the Feidong Complex exhibit low Al_2O_3 contents and A/CNK ratios, coupled with the absence of diagnostic S-type granite minerals (e.g., muscovite, cordierite) in thin section – features inconsistent with typical S-type granites (Chappell, 1992). These gneisses display elevated FeO^T/MgO ratios, Ga/Al ratios, total alkali contents, and low CaO contents, indicating geochemical affinities with A-type granites (Fig. 7a, b). Furthermore, the lack of inherited zircon grains permits the application of zircon saturation thermometry (T_{Zr}), which provides robust constraints on minimum magma crystallization temperatures (Miller et al., 2003; Watson and Harrison, 1983; Boehnke et al., 2013). Calculated T_{Zr} values (831–843 ℃) significantly exceed those of typical I-type granites (<800 ℃) and align with A-type granite signatures (Bonin, 2007), confirming the A-type classification of these granitic gneisses.

https://doi.org/10.5194/egusphere-2026-4742
Preprint. Discussion started: 2 September 2026

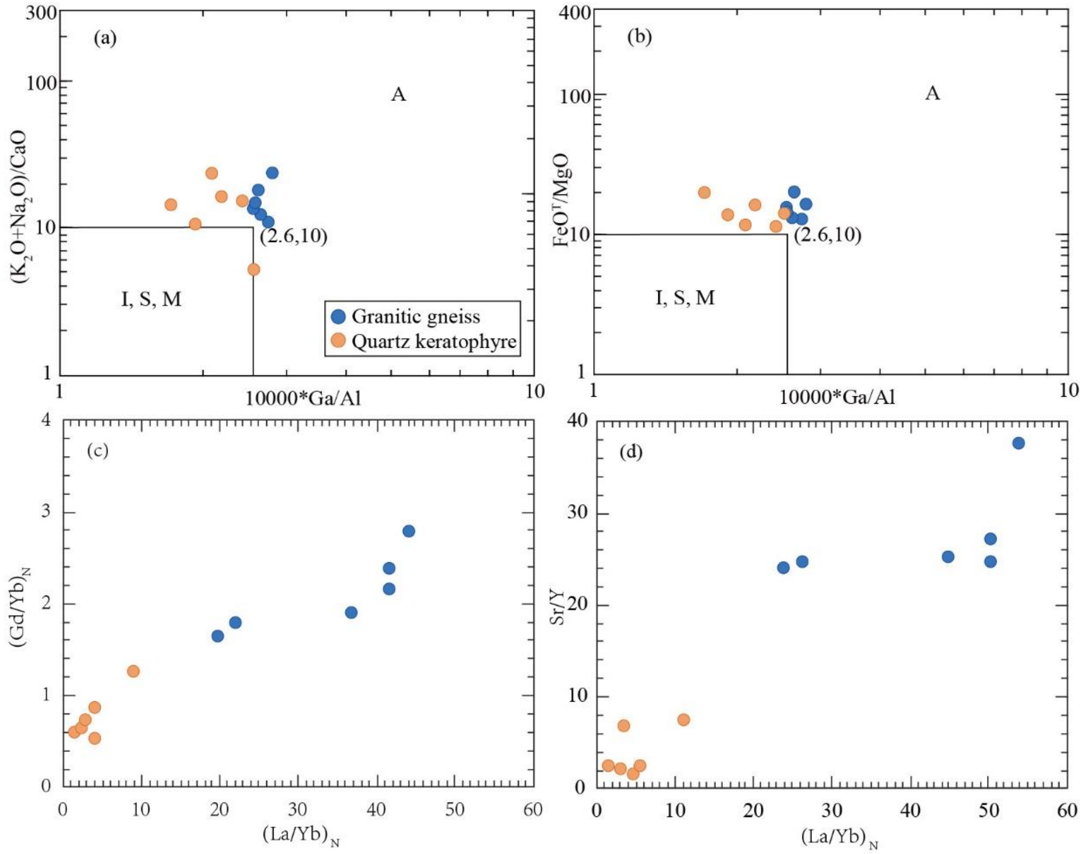

Figure 7: Granitic gneiss and quartz keratophyre samples in the Zhangbaling Uplift (a) $(K_2O+Na_2O)/CaO$ vs. Ga/Al; (b) FeO^T/MgO vs. Ga/Al; (c) $(Gd/Yb)_N$ vs. $(La/Yb)_N$; (d) Sr/Y vs. $(La/Yb)_N$.

Current genetic models for A-type granites include: (1) fractional crystallization of mantle-derived alkaline/tholeiitic basaltic magmas; (2) mixing between mantle-derived mafic and crustal felsic magmas; (3) partial melting of residual granulitic lower crust after extraction of I-/S-type magmas; and (4) direct partial melting of pre-existing ancient crustal materials (Whalen et al., 1987; Kerr and Fryer, 1993; Bonin, 2007). The restricted exposure of contemporaneous mafic rocks and absence of intermediate differentiates preclude a mantle fractionation origin in the study area. Furthermore, the lack of mafic enclaves, mineral resorption textures, and acicular apatite, combined with high SiO_2, low $Mg^{\#}$, Cr, and Ni contents in the gneisses, negate any significant role of crust-mantle magma mixing. Although Collins et al. (1982) proposed that high-temperature melting of residual felsic granulitic crust produces anhydrous melts with A-type signatures (e.g., enriched halogens, Zr, REE), the refractory nature of residual lower crustal granulites results in SiO_2 depletion during prior melting events. Such residues characteristically exhibit positive Ca anomalies, low K_2O/Na_2O, and low FeO^T/MgO ratios – features contradicting the high SiO_2, elevated K_2O/Na_2O, high FeO^T/MgO, and low CaO geochemistry observed here. Consequently, residual granulite melting contributions are negligible. Thus, the Feidong granitic gneisses are interpreted as products of partial melting of ancient crustal protoliths. These rocks exhibit high Sr/Y (24.68–37.68) and $(La/Yb)_N$ (21.72–44.44) ratios with pronounced HREE-depleted, right-sloping REE patterns (Fig. 7c, d), indicating garnet-dominated residual assemblages. Positive correlations between $(La/Yb)_N$ and both Sr/Y and $(Gd/Yb)_N$ ratios (Fig. 7c, d) corroborate garnet control due to its high HREE partition coefficients. Concomitantly, elevated Sr contents and subdued Eu anomalies indicate minimal plagioclase fractionation or retention (Fig. 5a, b). Zircon Hf isotopes reveal enriched signatures ($\varepsilon_{Hf}(t)$ = –16.9 to –10.6) with two-stage depleted mantle model ages (T_{DM2} = 2754–2335 Ma), indicating derivation from Paleoarchean–Paleoproterozoic crust. These results align with documented Archean–Paleoproterozoic magmatic and metamorphic events (Wang et al., 2016; Yuan et al., 2022a, b), supporting Neoproterozoic reworking of ancient Precambrian basement.

6.2 Petrogenesis of Zhangbaling quartz-keratophyre

The quartz keratophyre samples exhibit high $FeO^T/(FeO^T + MgO)$ ratios, elevated total alkali ($Na_2O + K_2O$ = 7.32–8.56 wt.%), and enriched high field strength element (HFSE) concentrations—characteristics consistent with typical A-type granite affinity (Whalen et al., 1987; Bonin, 2007). Discrimination diagrams confirm this classification, with all samples plotting within the A-type granite field (Fig. 7a, b). Notably, Ga/Al ratios in some quartz keratophyres ($1.70–2.55 \times 10^{-4}$) fall marginally below the A-type threshold ($>2.6 \times 10^{-4}$), reflecting lower values typically observed in subalkaline settings versus higher ratios in strongly peralkaline felsic rocks (Bonin, 2007). Additionally, low MgO (0.21–0.51 wt.%), Cr (0.98–6.04 ppm), and Ni (0.26–1.37 ppm) contents, coupled with mildly enriched zircon Hf isotopes ($\varepsilon_{Hf}(t)$ = –3.9 to 4.3), preclude significant mantle contributions, indicating derivation from a homogeneous continental crustal source.

Contrasting with the Feidong Neoproterozoic granitic gneisses, these quartz keratophyres feature: (1) higher HREE concentrations; (2) lower $(La/Yb)_N$ ratios (1.50–8.96); and (3) substantially reduced Sr/Y ratios (1.56–7.52). Such signatures imply a residual assemblage lacking garnet or rutile—minerals with high partition coefficients for HREEs. Pronounced negative Ba-Sr anomalies and low Eu/Eu values (0.34–0.66) further indicate plagioclase-dominated residues. Phase equilibrium constraints (Rapp and Watson, 1995) restrict melting depths to ≤33 km (≤1.0 GPa). Higher $\varepsilon_{Hf}(t)$ values and younger model ages (T_{DM2} = 1908–1396 Ma) distinguish these rocks from the Feidong suite's Archean sources, revealing a Paleoproterozoic–Mesoproterozoic crustal growth event linked to Columbia supercontinental assembly–breakup processes.

6.3 Petrogenesis of Zhangbaling spilites

Geochemical data from the Zhangbaling spilites reveal no systematic covariation of Ni contents or CaO/Al_2O_3 ratios with increasing MgO (Fig. 8a, b), indicating negligible fractionation of olivine and clinopyroxene. The absence of significant correlations between MgO and $Fe_2O_3^T/TiO_2$ concentrations (Fig. 8c, d) further precludes substantial fractionation of Fe-Ti oxides (magnetite or ilmenite). Elevated Eu/Eu* values and Sr contents collectively exclude plagioclase fractionation. Although Nb/U (4.5–47.8) and Nb/Ta ratios (11.4–36.6) reside within the compositional field bracketed by continental crust (Nb/U=10, Nb/Ta=12; Barth et al., 2000) and depleted MORB mantle (Nb/U=47, Nb/Ta=20; Münker et al., 2003), the lack of negative correlations between SiO_2 and these ratios (Fig. 8e, f) indicates these signatures represent inherent source characteristics rather than secondary processes. Furthermore, the absence of discernible xenocrystic zircons and pronounced

https://doi.org/10.5194/egusphere-2026-4742
Preprint. Discussion started: 2 September 2026

275 negative Zr-Hf anomalies in these mafic rocks rules out significant crustal contamination. Therefore, the magmatic evolution of the Zhangbaling spilites remained largely unaffected by fractional crystallization or crustal assimilation.

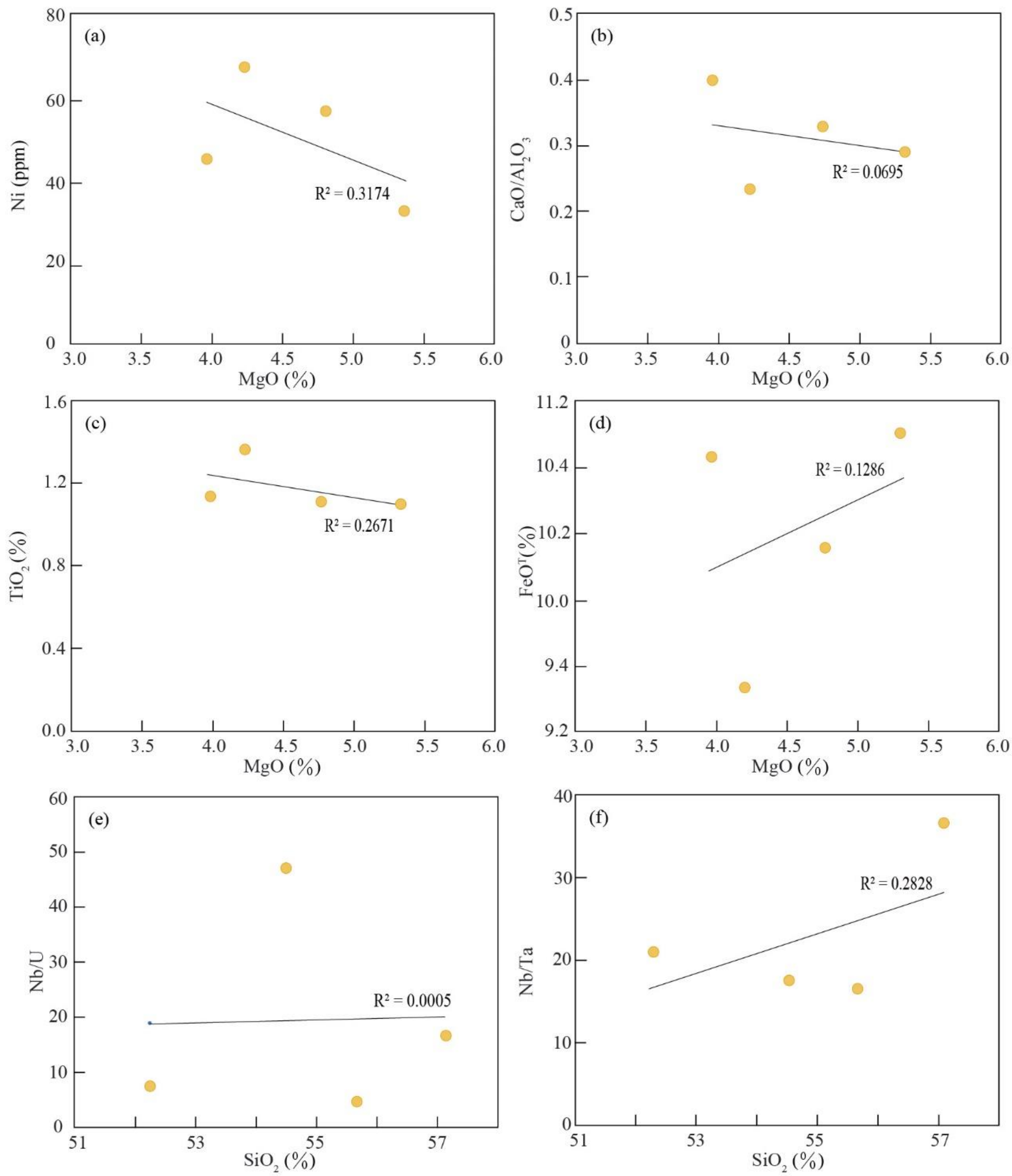

Figure 8: Spilite samples in the Zhangbaling Uplift (a) Ni vs. MgO; (b) CaO/Al_2O_3 vs. MgO; (c) TiO_2 vs. MgO; (d) FeO^T vs. MgO; (e) Nb/U vs. SiO_2; (f) Nb/Ta vs. SiO_2 diagram.

https://doi.org/10.5194/egusphere-2026-4742
Preprint. Discussion started: 2 September 2026

The Yangtze Craton experienced an extensional tectonic regime associated with Rodinia breakup during the mid-Neoproterozoic (808–730 Ma; e.g., He et al., 2018; Wu et al., 2020; Cai et al., 2021; Yuan et al., 2021, 2024), providing favorable conditions for asthenospheric upwelling. However, Zhangbaling spilites exhibit: (1) enriched light rare earth elements (LREEs), (2) relative enrichment of large-ion lithophile elements (LILEs: Rb, Ba, Pb), and (3) depletion of high-field-strength elements (HFSEs: Nb, Ta, Ti). These compositional features preclude direct derivation from asthenospheric or depleted OIB-source mantle. Discrimination plots of Nb/La vs. La/Yb and La/Ba vs. La/Nb confirm that all spilite samples deviate from asthenospheric and OIB mantle domains (Fig. 9a, b). Elevated La/Ta ratios (>30) in these mafic rocks are diagnostic of subcontinental lithospheric mantle affinities (Thompson and Morrison, 1988). Collectively, these data indicate that Neoproterozoic Zhangbaling mafic magmas originated from subduction-modified lithospheric mantle. Their arc-like geochemical signatures reflect prior melt/fluid metasomatism by melts and/or fluids derived from paleo-subducted slabs or recycled sedimentary materials.

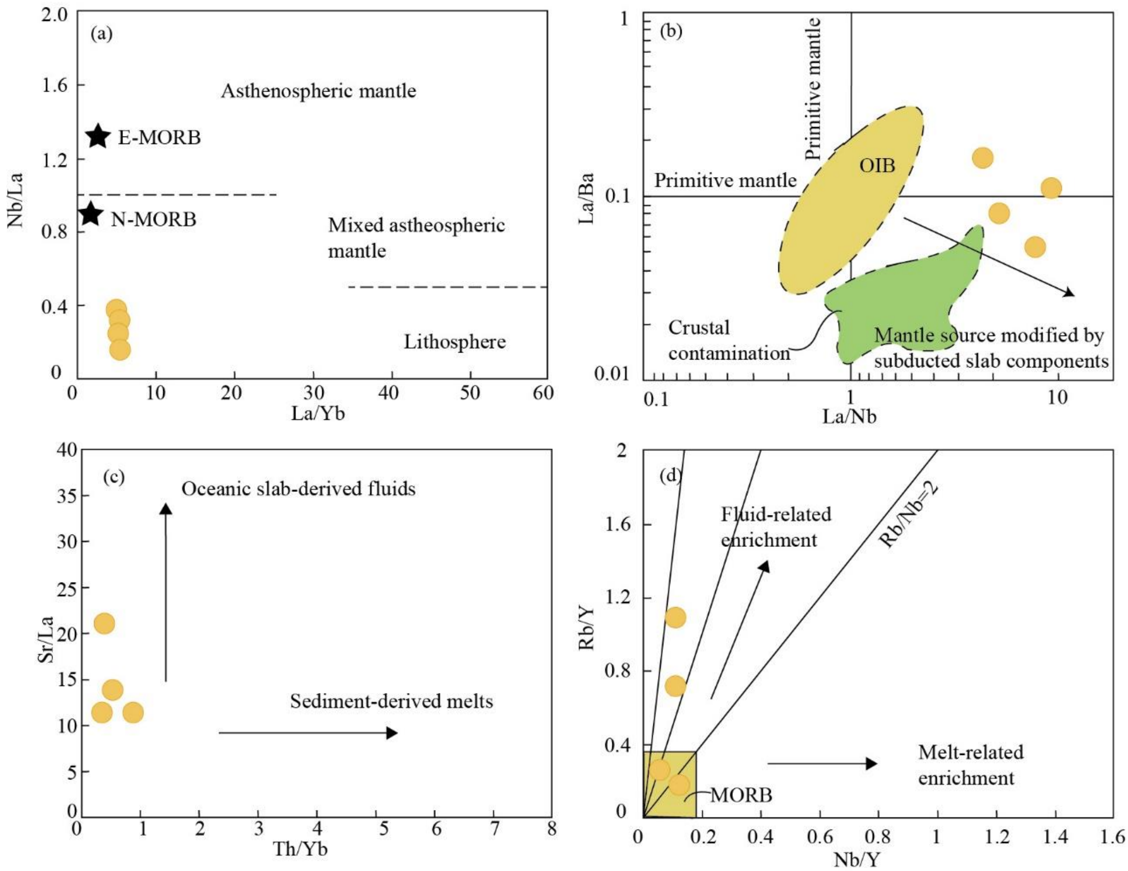

Figure 9: Spilite samples in the Zhangbaling Uplift (a) Nb/La vs.La/Yb; (b) La/Ba vs. La/Nb; (c) Sr/La vs. Th/Yb; (d) Rb/Y vs. Nb/Y diagram.

https://doi.org/10.5194/egusphere-2026-4742
Preprint. Discussion started: 2 September 2026

Metasomatism by fluids released from subducting slabs or melts derived from subducted sediments constitutes a fundamental mechanism for enriching the continental lithospheric mantle. Fluids generated during slab dehydration exhibit significant depletion in high-field-strength elements (HFSEs) while enriching fluid-mobile components such as large-ion lithophile elements (LILEs), Pb, Ba, and light rare earth elements (LREEs) (Elliott et al., 1997; Zhao and Zhou, 2009; Class et al., 2013). Conversely, slab melts display LREE and HFSE enrichment with characteristically low LILE/HFSE and LILE/LREE ratios (Defant and Drummond, 1990), coupled with elevated Nb/Zr and Nb/Y values (Kepezhinskas et al., 1997; Zhao and Asimow, 2014). The elevated LILEs/HFSEs ratios in spilite samples from the study area align with the slab-fluid metasomatic model. Their high Sr/La and low Th/Yb ratios further plot within the slab-fluid metasomatism field (Fig. 9c, d). Additionally, low Th/Y (0.02–0.08) and Th/Nb (0.28–0.46) ratios preclude a Th-enriched slab-melt metasomatized mantle source. Consequently, the arc-like geochemical signatures in these mafic intrusions originate from mantle metasomatism by subduction-derived fluids. Recent studies have identified middle Neoproterozoic mafic intrusions along the northern Yangtze margin, exemplified by the ~800 Ma Huangling dikes (Zhao et al., 2010) and 808 Ma Qichun pyroxenite cumulates (Zhang et al., 2016). These are commonly interpreted as products of early Neoproterozoic oceanic crust subduction and mantle metasomatism. This interpretation is reinforced by contemporaneous ophiolites and arc-affinity mafic igneous rocks exposed along the northern Yangtze Craton (Shi et al., 2007; Dong et al., 2011; Peng et al., 2012; Wang et al., 2016; Deng et al., 2017). Although reconnaissance of early Neoproterozoic magmatism remains sparse in the northeastern Yangtze margin, hindering definitive confirmation of subduction events, detrital zircon ages from the Haizhou Group quartz schist in the Sulu orogen (1074–902 Ma; Zhou et al., 2012) and the Meishan-Foziling groups within the Beihuaiyang unit (1000–900 Ma; Zhu et al., 2017) demonstrate that metasomatism triggered by late Mesoproterozoic to early Neoproterozoic subduction dominated the transformation of the primitive lithospheric mantle domain.

6.4 Implications for tectonic evolution

Recent research advances have significantly enhanced our understanding of the petrogenesis and tectonic setting of Neoproterozoic (particularly mid-Neoproterozoic) magmatic rocks in the Yangtze Craton. While it is widely accepted that their magmatic activity was governed by the Rodinia supercontinent breakup, substantial controversy persists regarding petrogenetic mechanisms and tectonic drivers, yielding multiple evolutionary models (Li et al., 2008, 2009; Zheng et al., 2008, 2013; Zhao et al., 2011; Zhao, 2015). Three dominant tectonic frameworks have emerged as principal explanatory paradigms: (1) Mantle Plume Model: This model constrains the amalgamation of the Yangtze and Cathaysia blocks (manifested by Jiangnan Orogen formation) at 1.1–0.9 Ga, constituting a Grenvillian orogenic event (Li et al., 2009). During this period, the Yangtze Craton occupied a central position within Rodinia. Intracontinental rifting initiated at 850–830 Ma, followed by intense plume-driven rifting between 830–745 Ma. This generated extensional systems including the Nanhua, Kangdian, and Bikou-Hannan rifts, accompanied by widespread mid-to-late Neoproterozoic bimodal magmatism of plume affinity. (2) Arc-Backarc Extension Model: Based on the identification of Neoproterozoic arc magmatic belts along the Yangtze margins (Jiangnan Orogen and Panxi-Hannan Arc; 1000–830 Ma; Zhou et al., 2002a, b, 2006a, b; Munteanu and Wilson, 2009; Dong

https://doi.org/10.5194/egusphere-2026-4742
Preprint. Discussion started: 2 September 2026

et al., 2012; Zhao and Asimow, 2014), this paradigm emphasizes calc-alkaline magmatism resulting from oceanic slab subduction. The 830 Ma ophiolites in the Jiangnan Orogen confirm subduction postdating Grenvillian orogenesis. Subsequent ongoing subduction induced backarc extension after 830 Ma, forming the volcanic-sedimentary sequence in the Nanhua Basin (Zhao et al., 2011, 2015). Consequently, the model reconstructs the Yangtze Craton along the periphery of Rodinia, flanked by an open ocean (Wang and Zhou, 2012b; Wang et al., 2013a, b; Zhou et al., 2006b; Du et al., 2014). (3) Intra-plate Rift Model: Proposing initial subduction during the late Mesoproterozoic (1.3–1.1 Ga), this model invokes arc-continent collision triggered by closure of a backarc basin in the early Neoproterozoic (960–860 Ma). Orogenic collapse during the mid-Neoproterozoic (830–800 Ma) facilitated emplacement of S-type granites (Zheng et al., 2007, 2008). The subsequent mid-late Neoproterozoic (780–740 Ma) witnessed extensive bimodal volcanism and low-$\delta^{18}O$ magmatism, recording peak rifting during Rodinia fragmentation (Zheng et al., 2004, 2007). Although these frameworks collectively provide critical insights into the Neoproterozoic evolution of the Yangtze Craton, none comprehensively resolves the inherent complexity of coeval magmatism and tectonic settings.

The Neoproterozoic rift setting along the northern Yangtze margin exhibits diagnostic incompatibility with mantle plume models: Critical evidence includes the absence of large-scale flood basalts (with total volcanic volume substantially lower than classical examples like the Siberian Traps), missing high-MgO magmatism (e.g., komatiites) and OIB-type mafic rocks with EMI/EMII endmember components, and lack of rapid siliceous hydrothermal deposits (e.g., chert layers) associated with plume-related thermal doming. The protracted magmatism (800–700 Ma) also argues against the plume model. Consequently, the dynamic mechanism of northern Yangtze rifting remains contested between subduction-backarc extension and continental rift models. Backarc extension necessitates spatiotemporal coupling with subduction zones, yet magmatic zircons from the Feidong Complex and Zhangbaling Group show no isotopic evidence for mid-Neoproterozoic juvenile crustal growth—contradicting backarc model predictions of coeval crustal accretion (~750 Ma) (Zhou et al., 2002a; Ling et al., 2003; Zhao and Zhou, 2009; Zhao et al., 2011; Dong et al., 2012). Furthermore, no Neoproterozoic high-pressure blueschists or other subduction-collision records exist to drive backarc extension. Integrated analysis of published and present data reveals voluminous A-type granite (800–700 Ma; e.g., Zheng et al., 2007, 2008; Zhang et al., 2013, 2019; Liu et al., 2015; Wu et al., 2019, 2020) whose spatiotemporal extent exceeds typical backarc systems. Sedimentary records additionally negate backarc models: while backarc basins characteristically display intercalated volcanic-sedimentary sequences with deepwater facies, this region exhibits only limited sedimentary strata (e.g., Beijiangjun Formation) during magmatic quiescence, devoid of diagnostic deepwater sedimentation. Conversely, high-angle normal fault systems inherent to rift settings intrinsically restrict extensive sediment accumulation, consistent with observed stratigraphy. Instead, high thermal gradients (1.0–3.5 kbar, 560–660 ℃) in rift environments provide optimal conditions for observed high-T/low-P metamorphism (He et al., 2018). Regional rock assemblages, magma source characteristics, and absence of intermediate rocks collectively align with lithospheric mantle partial melting coupled with incomplete fractionation in rift zones. Tectonic discrimination diagrams (Fig. 10) unambiguously indicate intraplate geochemical affinity. The spatiotemporally associated spilite-quartz keratophyre bimodal suite within the Zhangbaling Group likely represents an intracontinental rift product. Ultimately, dispersed multistage magmatism over >100

https://doi.org/10.5194/egusphere-2026-4742
Preprint. Discussion started: 2 September 2026

Myr correlates with protracted intracontinental extension while synchronizing with far-field stress fields during Rodinia breakup (approximately 750 Ma), establishing a genetic link between mid-Neoproterozoic extension and supercontinent-driven rifting.

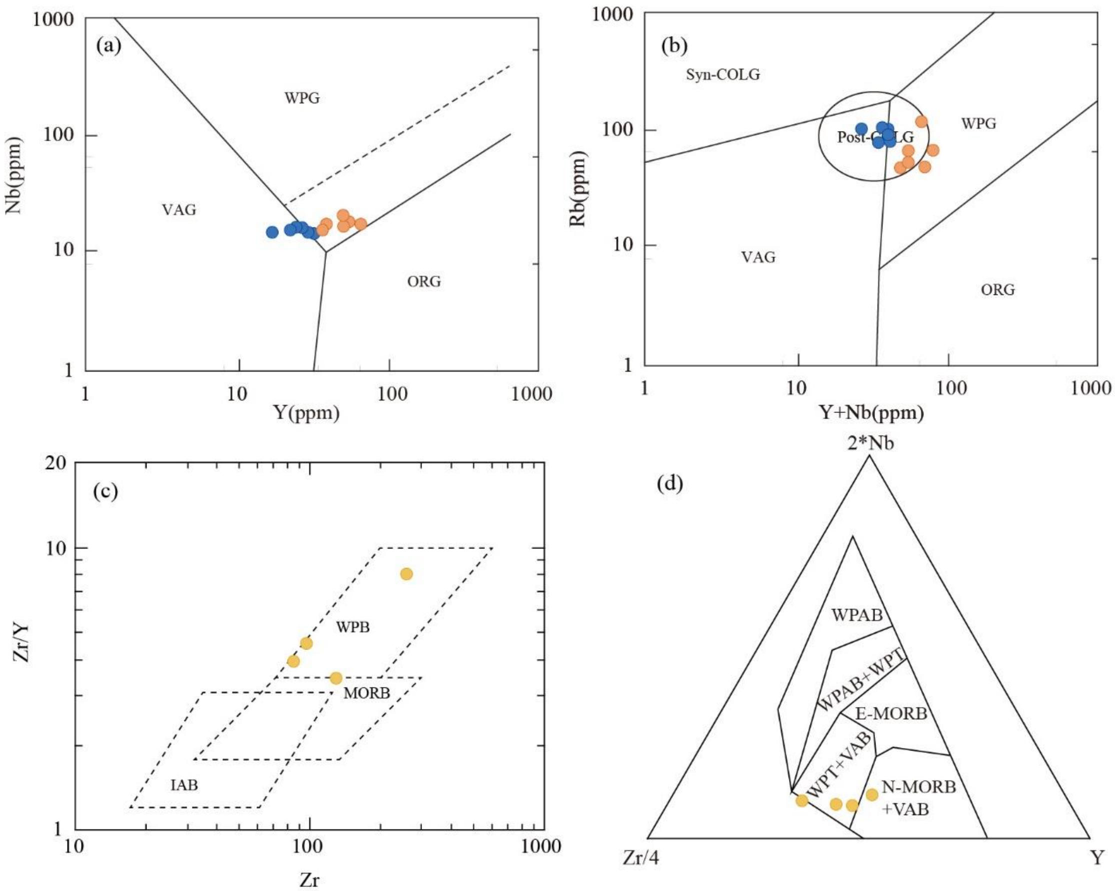

Figure 20: Rock samples from the Zhangbaling Uplift (a) Nb vs. Y; (b) Rb vs. Y+Nb; (c) Zr/Y vs. Zr; (d) 2*Nb vs. Zr/4 vs. Y diagram.

The Neoproterozoic magmatic events in the Zhangbaling Uplift of the northeastern Yangtze Craton provide critical constraints on a continental rift setting while establishing a definitive chronostratigraphic framework for its tectonic evolution. Early-stage magmatic emplacement in the Feidong region correlates with initial rifting. These granitic gneisses originated from partial melting of ancient lower crust within the garnet stability field (melting depths: 33–40 km). Coeval lithospheric extension triggered decompression melting of the mantle, inducing underplating of mantle-derived melts that facilitated lower crustal anatexis. Progressive rift development enabled sustained upwelling of mafic magmas, triggering extensive partial melting of the mid-upper crust at shallow depths (with plagioclase as the dominant residual phase) to form the Zhangbaling Group. Concurrent intense extension generated elevated geothermal gradients and enhanced crustal permeability, catalyzing the

https://doi.org/10.5194/egusphere-2026-4742
Preprint. Discussion started: 2 September 2026

development of meteoric water-dominated hydrothermal systems. This process drove pervasive oxygen isotope exchange in shallow crustal materials, resulting in systematic $\delta^{18}O$ depletion in Zhangbaling Group zircons (Cai et al., 2021; Yuan et al., 2021). Regional low-$\delta^{18}O$ magmatism across the northern Yangtze margin further attests to mature continental rift formation. Collectively, these magmatic records document a dynamic transition sequence from initial crustal extension to mature rift system development during Rodinia supercontinent breakup.

7 Conclusions

The Neoproterozoic magmatic rocks exposed along the northeastern Yangtze Craton can be chronologically subdivided into two distinct episodes based on zircon geochronology. Granitic gneisses from the Feidong Complex yield concordant U-Pb crystallization ages of 781–776 Ma, while bimodal volcanic rocks of the Zhangbaling Group are constrained to 753–730 Ma, exhibiting a spilite-quartz keratophyre lithological association. The Feidong granites display diagnostic A-type geochemical affinities, with garnet-dominated residual mineralogy in their magma source regions. This indicates petrogenesis through anatexis of ancient lower crust during the incipient rifting stage. In contrast, the development of the Zhangbaling bimodal volcanic succession marks a tectonic transition from initial crustal extension to a mature rift regime, comprehensively recording dynamical crustal extension processes accompanying the fragmentation of the Rodinia supercontinent.

Data availability

All new data generated as part of this study are included in data tables in supplement.

Author contributions

SW and XY: conceptualized and designed this study. SW and HY took part in data analysis. HY and XY led the geological interpretation. SW wrote the initial manuscript draft. All authors participated to the results discussion and approved the submission of this paper.

Competing interests

The contact author has declared that none of the authors has any competing interests.

Disclaimer

Publisher's note: Copernicus Publications remains neutral with regard to jurisdictional claims made in the text, published maps, institutional affiliations, or any other geographical representation in this paper. The authors bear the ultimate responsibility for providing appropriate place names. Views expressed in the text are those of the authors and do not necessarily reflect the views of the publisher.

Acknowledgements

We gratefully acknowledge Professor Hu Qiuyuan from Shandong Institute of Petroleum and Chemical Technology for his guidance on the tectonic aspects of this paper. We sincerely appreciate Lecturer Xia Lu from Shandong Institute of Petroleum and Chemical Technology for his instructive suggestions regarding the geochemical components of this study.

Financial support

This paper was financially supported by the National Natural Science Foundation of China (42302225).

References

Boehnke, P., Watson, E. B., Trail, D., Harrison, T. M., and Schmitt, A. K.: Zircon saturation re-revisited, Chem. Geol., 351, 324–334, https://doi.org/10.1016/j.chemgeo.2013.05.028, 2013.

Bonin, B.: A-type granites and related rocks: Evolution of a concept, problems and prospects, Lithos, 97, 1–29, https://doi.org/10.1016/j.lithos.2006.12.007, 2007.

Cai, Q. R., Niu, M. L., Yuan, X. Y., Wu, Q., Zhu, G., Li, X. C., Sun, Y., and Li, C.: Evidence for continental rifting from two episodes of mid-Neoproterozoic silicic magmatism in the northeastern Yangtze Block, China, Precambrian Res., 363, 106336, https://doi.org/10.1016/j.precamres.2021.106336, 2021.

Chappell, B. W. and White, A. J. R.: I- and S-type granites in the Lachlan Fold Belt, in: The Second Hutton Symposium on the Origin of Granites and Related Rocks, Geological Society of America Special Paper, 272, 1–26, https://doi.org/10.1130/SPE272-P1, 1992.

Class, C., Miller, D. M., Goldstein, S. L., and Langmuir, C. H.: Distinguishing melt and fluid subduction components in Umnak Volcanics, Aleutian Arc, Geochem. Geophys. Geosyst., 1, 1999GC000010, https://doi.org/10.1029/1999GC000010, 2000.

Collins, W. J., Beams, S. D., White, A. J. R., and Chappell, B. W.: Nature and origin of A-type granites with particular reference to southeastern Australia, Contrib. Mineral. Petrol., 80, 189–200, https://doi.org/10.1007/BF00374895, 1982.

Dalziel, I. W. D.: Pacific margins of Laurentia and East Antarctica-Australia as a conjugate rift pair: Evidence and implications for an Eocambrian supercontinent, Geology, 19, 598–601, https://doi.org/10.1130/0091-7613(1991)019%3C0598:PMOLAE%3E2.3.CO;2, 1991.

Defant, M. J. and Drummond, M. S.: Derivation of some modern arc magmas by melting of young subducted lithosphere, Nature, 347, 662–665, https://doi.org/10.1038/347662a0, 1990.

https://doi.org/10.5194/egusphere-2026-4742
Preprint. Discussion started: 2 September 2026

Deng, H., Peng, S., Polat, A., Kusky, T. M., Jiang, X. F., Han, Q. S., Wang, L., Huang, Y., Wang, J. P., Zeng, W., and Hu, Z. X.: Neoproterozoic IAT intrusion into Mesoproterozoic MOR Miaowan Ophiolite, Yangtze Craton: Evidence for evolving tectonic settings, Precambrian Res., 289, 75–94, https://doi.org/10.1016/j.precamres.2016.12.003, 2017.

Dong, Y. P., Liu, X. M., Santosh, M., Chen, Q., Zhang, X. N., Li, W., He, D. F., and Zhang, G. W.: Neoproterozoic accretionary tectonics along the northwestern margin of the Yangtze Block, China: Constraints from zircon U-Pb geochronology and geochemistry, Precambrian Res., 196–197, 247–274, https://doi.org/10.1016/j.precamres.2011.12.007, 2012.

Dong, Y. P., Liu, X. M., Santosh, M., Zhang, X. N., Chen, Q., Yang, C., and Yang, Z.: Neoproterozoic subduction tectonics of the northwestern Yangtze Block in South China: Constraints from zircon U-Pb geochronology and geochemistry of mafic intrusions in the Hannan Massif, Precambrian Res., 189, 66–90, https://doi.org/ 10.1016/j.precamres.2011.05.002, 2011.

Elliott, T., Plank, T., Zindler, A., White, W., and Bourdon, B.: Element transport from slab to volcanic front at the Mariana arc, J. Geophys. Res., 102, 14991–15019, https://doi.org/10.1029/97JB00788, 1997.

Gao, S., Yang, J., Zhou, L., Li, M., Hu, Z. C., and Guo, J. L.: Age and growth of the Archean Kongling terrain, South China, with emphasis on 3.3 Ga granitoid gneisses, Am. J. Sci., 311, 153–182, https://doi.org/10.2475/02.2011.03, 2011.

He, Q., Zhang, S. B., and Zheng, Y. F.: Evidence for regional metamorphism in a continental rift during the Rodinia breakup, Precambrian Res., 314, 414–427, https://doi.org/10.1016/j.precamres.2018.06.009, 2018.

Hoffman, P. F.: Did the breakout of Laurentia turn Gondwanaland inside-out ?, Science, 252, 1409–1412, https://doi.org/10.1126/science.252.5011.1409, 1991.

Jiang, X. F., Peng, S. B., Polat, A., Kusky, T., Wang, L., and Wu, T. Y.: Geochemistry and geochronology of mylonitic metasedimentary rocks associated with the Proterozoic Miaowan Ophiolite Complex, Yangtze Craton, China: Implications for geodynamic events, Precambrian Res., 279, 37–56, https://doi.org/10.1016/j.precamres.2016.04.004, 2016.

Kang, T., Liu, X. Y., Wang, J., Nie, F., and Shi, Y. H.: Analysis of metamorphic attribution and geochronology for the Feidong Terrane in the east of the Tan-Lu Fault, Acta Petrol. Sin., 29, 3142–3158, http://www.ysxb.ac.cn/en/article/id/aps_20130915, 2013.

Kepezhinskas, P., McDermott, F., Defant, M. J., Hochstaedter, A., Drummond, M. S., Hawkesworth, C. J., Koloskov, A., Maury, R. C., and Bellon, H.: Trace element and Sr-Nd-Pb isotopic constraints on a three-component model of Kamchatka Arc petrogenesis, Geochim. Cosmochim. Acta, 61, 577–600, https://doi.org/10.1016/S0016-7037(96)00349-3, 1997.

Kerr, A. and Fryer, B. J.: Nd isotope evidence for crust-mantle interaction in the generation of A-type granitoid suites in Labrador, Canada, Chem. Geol., 104, 39–60, https://doi.org/10.1016/0009-2541(93)90141-5, 1993.

Li, X. H., Li, W. X., and He, B.: Building of the South China Block and its relevance to assembly and breakup of Rodinia supercontinent: Observations, interpretations and tests, Bull. Mineral. Petrol. Geochem., 31, 543–559, https://doi.org/10.0000/BMPG.1007-2802.2012-i6-02, 2012.

Li, X. H., Li, W. X., Li, Z. X., Lo, C. H., Wang, J., Ye, M. F., and Yang, Y. H.: Amalgamation between the Yangtze and Cathaysia Blocks in South China: Constraints from SHRIMP U-Pb zircon ages, geochemistry and Nd-Hf isotopes of the Shuangxiwu volcanic rocks, Precambrian Res., 174, 117–128, https://doi.org/10.1016/j.precamres.2009.07.004, 2009.

Li, Z. X., Bogdanova, S. V., Collins, A. S., Davidson, A., De Waele, B., Ernst, R. E., Fitzsimons, I. C. W., Fuck, R. A., Gladkochub, D. P., Jacobs, J., Karlstrom, K. E., Lu, S., Natapov, L. M., Pease, V., Pisarevsky, S. A., Thrane, K., and Vernikovsky, V.: Assembly, configuration, and break-up history of Rodinia: A synthesis, Precambrian Res., 160, 179–210, https://doi.org/10.1016/j.precamres.2007.04.021, 2008.

Li, Z. X., Li, X. H., Kinny, P. D., and Wang, J.: The breakup of Rodinia: Did it start with a mantle plume beneath South China?, Earth Planet. Sci. Lett., 173, 171–181, https://doi.org/10.1016/S0012-821X(99)00240-X, 1999.

Ling, W. L., Gao, S., and Zhang, B.: Neoproterozoic tectonic evolution of the northwestern Yangtze Craton, South China: Implications for amalgamation and break-up of the Rodinia Supercontinent, Precambrian Res., 122, 111–140, https://doi.org/10.1016/S0301-9268(02)00222-X, 2003.

Liou, J. G., Wang, X., and Choi, S. Y.: Alkali amphiboles from Late Archean gneiss of the Wuhe Group, Anhui, central China: Not an indication of high P/T metamorphism, Acta Petrol. Mineral., 11, 205–224, https://www.yskw.ac.cn/yskwxzz/article/abstract/19920333, 1992.

Liu, L., Yang, X. Y., Santosh, M., Zhou, H. Y., Geng, J. Z., and Sun, W. D.: Neoproterozoic intraplate crustal accretion on the northern margin of the Yangtze Block: Evidence from geochemistry, zircon SHRIMP U-Pb dating and Hf isotopes from the Fuchashan Complex, Precambrian Res., 268, 97–114, doi.org/10.1016/j.precamres.2015.07.004, 2015.

Ludwig, K. R.: Isoplot 3.00: A geochronological toolkit for Microsoft Excel, Berkeley Geochronology Center Special Publication No. 4, Berkeley, 74, https://www.bgc.org/isoplot, 2003.

McMenamin, M. A. S. and McMenamin, D. L. S.: The emergence of animals: The Cambrian breakthrough, Columbia University Press, New York, USA, 217, https://cup.columbia.edu/book/the-emergence-of-animals/9780231066471/, 1990.

Miller, C. F., McDowell, S. M., and Mapes, R. W.: Hot and cold granites? Implications of zircon saturation temperatures and preservation of inheritance, Geology, 31, 529–532, https://doi.org/10.1130/0091-7613(2003)031<0529:HACGIO>2.0.CO;2, 2003.

Moores, E. M.: Southwest U.S.-East Antarctic (SWEAT) connection: A hypothesis, Geology, 19, 425–428, https://doi.org/10.1130/0091-7613(1991)019%3C0425:SUSEAS%3E2.3.CO;2, 1991.

Münker, C., Pfänder, J. A., Weyer, S., Büchl, A., Kleine, T., and Mezger, K.: Evolution of planetary cores and the Earth-Moon system from Nb/Ta systematics, Science, 301, 84–87, https://doi.org/10.1126/science.1084662, 2003.

Munteanu, M. and Wilson, A.: The South China piece in the Rodinian puzzle, Precambrian Res., 171, 74–76, https://doi.org/10.1016/j.precamres.2009.01.009, 2009.

Nie, F., Shi, Y. H., Zhang, Z. B., Wang, J., and Cao, S.: The initial time of the Tan-Lu wrench fault: In the view of geochronological data of the basement rocks, northern Anhui Province, Chin. Sci. Bull., 60, 2315–2326, https://doi.org/10.1360/N972015-00349, 2015.

Peng, S. B., Kusky, T. M., Jiang, X. F., Wang, L., Wang, J. P., and Deng, H.: Geology, geochemistry, and geochronology of the Miaowan ophiolite, Yangtze Craton: Implications for South China's amalgamation history with the Rodinian supercontinent, Gondwana Res., 21, 577–594, https://doi.org/10.1016/j.gr.2011.07.010, 2012.

Rapp, R. P. and Watson, E. B.: Dehydration melting of metabasalt at 8–32 kbar: Implications for continental growth and crust-mantle recycling, J. Petrol., 36, 891–931, https://doi.org/10.1093/petrology/36.4.891, 1995.

Shi, Y. H.: Petrology and zircon U-Pb geochronology of metamorphic massifs around the middle segment of the Tan-Lu fault to define the boundary between the North and South China blocks, J. Asian Earth Sci., 141, 140–160, https://doi.org/10.1016/j.jseaes.2016.07.001, 2016.

Shi, Y. R., Liu, D. Y., and Zhang, Z. Q.: SHRIMP zircon U-Pb dating of gabbro and granite from the Huashan ophiolite, Qinling Orogenic Belt, China: Neoproterozoic suture on the northern margin of the Yangtze Craton, Acta Geol. Sin.-Engl., 81, 239–243, https://doi.org/10.1111/j.1755-6724.2007.tb00947.x, 2007.

Thompson, R. N. and Morrison, M. A.: Asthenospheric and lower-lithospheric mantle contributions to continental extensional magmatism: An example from the British Tertiary Province, Chem. Geol., 68, 1–15, https://doi.org/10.1016/0009-2541(88)90082-4, 1988.

Wang, J., Deng, Q., and Wang, Z. J.: New evidences for sedimentary attributes and timing of the “Macaoyuan conglomerates” on the northern margin of the Yangtze Block in southern China, Precambrian Res., 235, 58–70, https://doi.org/10.1016/j.precamres.2013.06.003, 2013.

Wang, W., Cawood, P. A., Zhou, M. F., and Zhao, J. H.: Paleoproterozoic magmatic and metamorphic events link Yangtze to northwest Laurentia in the Nuna supercontinent, Earth Planet. Sci. Lett., 433, 269–279, https://doi.org/10.1016/j.epsl.2015.11.005, 2016.

Wang, W. and Zhou, M. F.: Sedimentary records of the Yangtze Block (South China) and their correlation with equivalent Neoproterozoic sequences on adjacent continents, Sediment. Geol., 265–266, 126–142, https://doi.org/10.1016/j.sedgeo.2012.04.003, 2012.

Wang, W., Zhou, M. F., Yan, D. P., Li, L., and Malpas, J.: Detrital zircon record of Neoproterozoic active-margin sedimentation in the eastern Jiangnan Orogen, South China, Precambrian Res., 235, 1–19, https://doi.org/10.1016/j.precamres.2013.05.013, 2013.

Watson, E. B. and Harrison, T. M.: Zircon saturation revisited: Temperature and composition effects in a variety of crustal magma types, Earth Planet. Sci. Lett., 64, 295–304, https://doi.org/10.1016/0012-821X(83)90211-X, 1983.

Wei, Y. X., Peng, S. B., Jiang, X. F., Peng, Z. Q., Peng, L. H., and Li, Z. H.: SHRIMP zircon U-Pb ages and geochemical characteristics of the Neoproterozoic granitoids in the Huangling anticline and its tectonic setting, J. Earth Sci., 23, 659–675, https://doi.org/10.1007/s12583-012-0284-z, 2012.

Whalen, J. B., Currie, K. L., and Chappell, B. W.: A-type granites: Geochemical characteristics, discrimination and petrogenesis, Contrib. Mineral. Petrol., 95, 407–419, https://doi.org/10.1007/BF00402202, 1987.

Wu, P., Zhang, S. B., and Zheng, Y. F.: Amalgamation of South China into Rodinia during the Grenvillian accretionary orogeny: Geochemical evidence from Early Neoproterozoic igneous rocks in the northern margin of the South China Block, Precambrian Res., 321, 221–243, https://doi.org/10.1016/j.precamres.2018.12.015, 2019.

Wu, P., Zhang, S. B., Zheng, Y. F., Li, Q. L., and Sun, F. Y.: The occurrence of Neoproterozoic low δ18O igneous rocks in the northwestern margin of the South China Block: Implications for the Rodinia configuration, Precambrian Res., 347, 105841, https://doi.org/10.1016/j.precamres.2020.105841, 2020.

Wu, R. X., Zheng, Y. F., Wu, Y. B., Zhao, Z. F., Zhang, S. B., Liu, X., and Wu, F. Y.: Reworking of juvenile crust: Element and isotope evidence from Neoproterozoic granodiorite in South China, Precambrian Res., 146, 179–212, https://doi.org/10.1016/j.precamres.2006.01.012, 2006.

Xu, J. W., Zhu, G., Tong, W. X., Cui, K. R., and Liu, Q.: Formation and evolution of the Tancheng-Lujiang wrench fault system: A major shear system to the northwest of the Pacific Ocean, Tectonophysics, 134, 273–310, https://doi.org/10.1016/0040-1951(87)90342-8, 1987.

Xu, X. B., Xue, D. J., Li, Y., Hu, P., and Chen, N. S.: Neoproterozoic sequences along the Dexing-Huangshan fault zone in the eastern Jiangnan Orogen, South China: Geochronological and geochemical constraints, Gondwana Res., 25, 368–382, https://doi.org/10.1016/j.gr.2013.03.020, 2014.

Xia, L. Q., Xia, Z. C., Xu, X. Y., Li, X. G., and Ma, Z. P.: Mid-Late Neoproterozoic rift-related volcanic rocks in China: Geological records of rifting and break-up of Rodinia, Geosci. Front., 3, 375–399, https://doi.org/10.1016/j.gsf.2011.10.004, 2012.

Yang, Z. N., Yang, K. G., Xu, Y., Deng, X., Cheng, W. Q., and Long, Z. Y.: Zircon U-Pb geochronology, Hf isotopic composition, and geological implications of the Neoproterozoic meta-sedimentary rocks in Suizhou-Zaoyang area, the northern Yangtze Block, Sci. China Earth Sci., 58, 1910–1923, https://doi.org/10.1007/s11430-015-5073-y, 2015.

Yuan, X. Y., Niu, M. L., Cai, Q. R., Wu, Q., Zhu, G., Li, X. C., Sun, Y., and Li, C.: Bimodal volcanic rocks in the northeastern margin of the Yangtze Block: Response to breakup of Rodinia supercontinent, Lithos, 390–391, 106108, https://doi.org/10.1016/j.lithos.2021.106108, 2021.

Yuan, X. Y., Niu, M. L., Cai, Q. R., Zhu, G., Wu, Q., Li, X. C., Sun, Y., and Li, C.: The implication of two episodic Precambrian supercontinent convergence events from enriched mantle beneath the Yangtze Block: Constraints from the Zhangbaling mafic rocks, Precambrian Res., 371, 106561, https://doi.org/10.1016/j.precamres.2022.106561, 2022.

Yuan, X. Y., Niu, M. L., Cai, Q. R., Zhu, G., Wu, Q., Li, X. C., Sun, Y., Li, C., and Qian, T.: The nature of Paleoproterozoic basement in the northern Yangtze and its geological implication, Precambrian Res., 378, 106761, https://doi.org/10.1016/j.precamres.2022.106761, 2022.

Yuan, X. Y., Niu, M. L., Cai, Q. R., Zhu, G., and Wu, Q.: The nature of Neoproterozoic magmatism in the northeastern Yangtze Craton: Implications for breakup of Rodinia supercontinent, Precambrian Res., 405, 107353, https://doi.org/10.1016/j.precamres.2024.107353, 2024.

Zhang, Q., Teyssier, C., and Jim, D.: Oblique collision between North and South China recorded in Zhangbaling and Fuchashan (Dabie-Sulu transfer zone), Geol. Soc. Am. Spec. Pap., 434, 167–206, https://doi.org/10.1130/2007.2434(09), 2007.

https://doi.org/10.5194/egusphere-2026-4742
Preprint. Discussion started: 2 September 2026

Zhang, S. B., Wu, R. X., and Zheng, Y. F.: Neoproterozoic continental accretion in South China: Geochemical evidence from the Fuchuan ophiolite in the Jiangnan Orogen, Precambrian Res., 220–221, 45–64, https://doi.org/10.1016/j.precamres.2012.07.010, 2012.

Zhang, S. B., Wu, P., and Zheng, Y. F.: Mafic magmatic records of Rodinia amalgamation in the northern margin of the South China Block, Earth Sci., 44, 4157–4166, https://doi.org/10.3799/dqkx.2019.252, 2019.

Zhang, S. B. and Zheng, Y. F.: Formation and evolution of Precambrian continental lithosphere in South China, Gondwana Res., 23, 1241–1260, https://doi.org/10.1016/j.gr.2012.09.005, 2013.

Zhang, S. B., Zheng, Y. F., Zhao, Z. F., Wu, Y. B., Yuan, H. L., and Wu, F. Y.: Origin of TTG-like rocks from anatexis of ancient lower crust: Geochemical evidence from Neoproterozoic granitoids in South China, Lithos, 113, 347–368, https://doi.org/10.1016/j.lithos.2009.04.024, 2009.

Zhao, G. C.: Jiangnan Orogen in South China: Developing from divergent double subduction, Gondwana Res., 27, 1173–1180, https://doi.org/10.1016/j.gr.2014.09.004, 2015.

Zhao, J. H. and Asimow, P. D.: Neoproterozoic boninite-series rocks in South China: A depleted mantle source modified by sediment-derived melt, Chem. Geol., 388, 98–111, https://doi.org/10.1016/j.chemgeo.2014.09.004, 2014.

Zhao, J. H. and Zhou, M. F.: Neoproterozoic adakitic plutons in the northern margin of the Yangtze Block, China: Partial melting of a thickened lower crust and implications for secular crustal evolution, Lithos, 104, 231–248, https://doi.org/10.1016/j.lithos.2007.12.009, 2008.

Zhao, J. H. and Zhou, M. F.: Secular evolution of the Neoproterozoic lithospheric mantle underneath the northern margin of the Yangtze Block, South China, Lithos, 107, 152–168, https://doi.org/10.1016/j.lithos.2008.09.017, 2009.

Zhao, J. H. and Zhou, M. F.: Neoproterozoic high-Mg basalts formed by melting of ambient mantle in South China, Precambrian Res., 233, 193–205, https://doi.org/10.1016/j.precamres.2013.04.017, 2013.

Zhao, J. H., Zhou, M. F., and Zheng, J. P.: Constraints from zircon U-Pb ages, O and Hf isotopic compositions on the origin of Neoproterozoic peraluminous granitoids from the Jiangnan Fold Belt, South China, Contrib. Mineral. Petrol., 166, 1505–1519, https://doi.org/10.1007/s00410-013-0940-z, 2013a.

Zhao, J. H., Zhou, M. F., Yan, D. P., Zheng, J. P., and Li, J. W.: Reappraisal of the ages of Neoproterozoic strata in South China: No connection with the Grenvillian orogeny, Geology, 39, 299–302, https://doi.org/10.1130/G31701.1, 2011.

Zhao, J. H., Zhou, M. F., and Zheng, J. P.: Metasomatic mantle source and crustal contamination for the formation of the Neoproterozoic mafic dike swarm in the northern Yangtze Block, South China, Lithos, 115, 177–189, https://doi.org/10.1016/j.lithos.2009.12.001, 2010.

Zhao, T., Zhu, G., Lin, S. Z., Yan, L. J., and Jiang, Q. Q.: Protolith ages and deformation mechanism of metamorphic rocks in the Zhangbaling Uplift segment of the Tan-Lu Fault Zone, Sci. China Earth Sci., 57, 2740–2757, https://doi.org/10.1007/s11430-014-4959-4, 2014.

https://doi.org/10.5194/egusphere-2026-4742
Preprint. Discussion started: 2 September 2026

Zheng, Y. F., Gong, B., Zhao, Z. F., Wu, Y. B., and Chen, F. K.: Zircon U-Pb age and O isotope evidence for Neoproterozoic low-18O magmatism during supercontinental rifting in South China: Implications for the snowball Earth event, Am. J. Sci., 308, 484–516, https://doi.org/10.2475/04.2008.04, 2008a.

Zheng, Y. F., Fu, B., Gong, B., and Li, L.: Stable isotope geochemistry of ultrahigh pressure metamorphic rocks from the Dabie-Sulu Orogen in China: Implications for geodynamics and fluid regime, Earth-Sci. Rev., 62, 105–161, https://doi.org/10.1016/S0012-8252(02)00133-2, 2003.

Zheng, Y. F., Wu, R. X., Wu, Y. B., Zhang, S. B., Yuan, H., and Wu, F. Y.: Rift melting of juvenile arc-derived crust: Geochemical evidence from Neoproterozoic volcanic and granitic rocks in the Jiangnan Orogen, South China, Precambrian Res., 163, 351–383, https://doi.org/10.1016/j.precamres.2008.01.004, 2008.

Zheng, Y. F., Wu, Y. B., and Chen, F. K.: Zircon U-Pb and oxygen isotope evidence for a large-scale 18O depletion event in igneous rocks during the Neoproterozoic, Geochim. Cosmochim. Acta, 68, 4145–4165, https://doi.org/10.1016/j.gca.2004.01.007, 2004.

Zheng, Y. F., Wu, Y. B., Gong, B., Chen, R. X., Tang, J., and Zhao, Z. F.: Tectonic driving of Neoproterozoic glaciations: Evidence from extreme oxygen isotope signature of meteoric water in granite, Earth Planet. Sci. Lett., 256, 196–210, https://doi.org/10.1016/j.gca.2004.01.007, 2007.

Zheng, Y. F., Xiao, W. J., and Zhao, G. C.: Introduction to tectonics of China, Gondwana Res., 23, 1189–1206, https://doi.org/10.1016/j.gr.2012.10.001, 2013.

Zheng, Y. F., Zhang, S. B., Zhao, Z. F., Wu, Y. B., Li, X., Li, Z., and Wu, F. Y.: Contrasting zircon Hf and O isotopes in the two episodes of Neoproterozoic granitoids in South China: Implications for growth and reworking of continental crust, Lithos, 96, 127–150, https://doi.org/10.1016/j.lithos.2006.10.003, 2007b.

Zhou, J. B., Simon, A. W., Liu, F. L., and Han, J.: Zircon U-Pb and Lu-Hf isotope study of the Neoproterozoic Haizhou Group in the Sulu Orogen: Provenance and tectonic implications, Lithos, 136–139, 261–281, https://doi.org/10.1016/j.lithos.2011.01.015, 2012.

Zhou, M. F., Kennedy, A. K., Sun, M., Mapes, J., and Lesher, C. M.: Neoproterozoic arc-related mafic intrusions along the northern margin of South China: Implications for the accretion of Rodinia, J. Geol., 110, 611–618, https://doi.org/10.1086/341762, 2002.

Zhou, M. F., Yan, D. P., Kennedy, A. K., Li, Y. Q., and Ding, J.: SHRIMP U-Pb zircon geochronological and geochemical evidence for Neoproterozoic arc-magmatism along the western margin of the Yangtze Block, South China, Earth Planet. Sci. Lett., 196, 51–67, https://doi.org/10.1016/S0012-821X(01)00595-7, 2002.

Zhou, M. F., Ma, Y.X., Yan, D. P., Xia, X., Zhao, J. H., and Sun, M.: The Yanbian Terrane (southern Sichuan Province, SW China): A Neoproterozoic arc assemblage in the western margin of the Yangtze Block, Precambrian Res., 144, 19–38, https://doi.org/10.1016/j.precamres.2005.11.002, 2006.

https://doi.org/10.5194/egusphere-2026-4742
Preprint. Discussion started: 2 September 2026

Zhou, M. F., Yan, D. P., Wang, C. L., Qi, L., and Kennedy, A. K.: Subduction-related origin of the 750 Ma Xuelongbao adakitic complex (Sichuan Province, China): Implications for the tectonic setting of the giant Neoproterozoic magmatic event in South China, Earth Planet. Sci. Lett., 248, 286–300, https://doi.org/10.1016/j.epsl.2006.05.032, 2006.

Zhu, G., Liu, C., Gu, C. C., Zhang, S., Li, Y. J., and Su, N.: Oceanic plate subduction history in the western Pacific Ocean: Constraint from Late Mesozoic evolution of the Tan-Lu Fault Zone, Sci. China Earth Sci., 61, 386–405, https://doi.org/10.1007/s11430-017-9136-4, 2018.

Zhu, G., Niu, M. L., Xie, C. L., and Wang, Y. S.: Sinistral to normal faulting along the Tan-Lu Fault Zone: Evidence for geodynamic switching of the East China continental margin, J. Geol., 118, 277–293, https://doi.org/10.1086/651540, 2010.

Zhu, G., Song, C. Z., Wang, D. X., Liu, G. S., and Xu, J. W.: Studies on $^{40}Ar/^{39}Ar$ thermochronology of strike-slip time of the Tan-Lu Fault Zone and their tectonic implications, Sci. China Ser. D, 44, 1002–1009, https://doi.org/10.1007/BF02875393, 2005.

Zhu, G., Wang, Y. S., Wang, W., Zhang, S., Liu, C., Gu, C. C., and Li, Y. J.: An accreted micro-continent in the north of the Dabie Orogen, East China: Evidence from detrital zircon dating, Tectonophysics, 698, 47–64, https://doi.org/10.1016/j.tecto.2017.01.004, 2017.

Zong, K. Q., Klemd, R., Yuan, Y., He, Z. Y., Guo, J. L., Shi, X. L., Liu, Y. S., Hu, Z. C., and Zhang, Z. M.: The assembly of Rodinia: The correlation of early Neoproterozoic (ca. 900 Ma) high-grade metamorphism and continental arc formation in the southern Beishan Orogen, southern Central Asian Orogenic Belt (CAOB), Precambrian Res., 290, 32–48, https://doi.org/10.1016/j.precamres.2016.12.010, 2017.